



# Assessing the degree of soil salinity in the Indian Sundarban Biosphere Reserve using measured soil electrical conductivity and remote sensing data-derived salinity indices

Mehebab Sahana<sup>1</sup> · Sufia Rehman<sup>2</sup> · Priyank Pravin Patel<sup>3</sup> · Jie Dou<sup>4</sup> · Haoyuan Hong<sup>5</sup> · Haroon Sajjad<sup>2</sup> 

Received: 18 August 2019 / Accepted: 28 November 2020 / Published online: 3 January 2021  
© Saudi Society for Geosciences 2021

## Abstract

The Sundarban Biosphere Reserve (SBR) in India is vulnerable to soil salinity issues arising out of the occurrence of regular floods and storm surges. While much research has investigated various geo-hazards in this Reserve, the soil salinity aspect has remained underemphasized. This study assesses the degree of soil salinity and its spatial distribution in the SBR, using remote sensing and field measured datasets. Eight soil salinity indices extracted from satellite images were statistically correlated with measured electrical conductivity values using the Pearson correlation coefficient. Through this, the Salinity Index (SI-3) and the Normalized Difference Soil Index (NDSI) were determined as the most suitable indices to map the SBR's soil salinity. The spatial analysis of these indices revealed that the administrative Blocks of Patharpratima, Basanti, Kultali, Sagar, Sandeshkhali-I, Gosaba, and Haroa experienced extremely high level of soil salinity and salt intrusion. The high drainage density and close proximity of these blocks to rivers fosters such high soil salinity. The study calls for efficacious policy measures to lessen the effects of soil salinity on the subsistence prospects of the coastal communities. The methodology adopted in this study can be utilized for similar analysis in other saline-affected areas at various spatial scales.

**Keywords** Salinization · Electrical conductivity · Soil salinity indices · Remote sensing · SBR

## Introduction

Salinization occurs through the accumulation and increasing concentration of salts in the soil layer and is the main cause of

land degradation in coastal areas (Shrestha 2006; Daliakopoulos et al. 2016). Soil salinity is a serious threat to agricultural activities along coastlines (Jingwei et al. 2008). It alters the local soil chemistry and often causes decrease in

## Highlights

- Soil samples were collected for measuring the electrical conductivity (EC).
- Correlation matrix was run to select a suitable spectral soil salinity index.
- Degree of salinity was determined by interpolating computed salinity index values.
- Extremely high salinity (EC > 8.0 dS/m) along coast and quite high (6–8 dS/m) inland.
- Proximity to drainage network and higher drainage density influenced soil salinity.

Responsible Editor: Stefan Grab

✉ Haroon Sajjad  
haroon.geog@gmail.com

<sup>1</sup> School of Environment, Education & Development, University of Manchester, Manchester, UK

<sup>2</sup> Department of Geography, Jamia Millia Islamia, Jamia Nagar, New Delhi, India

<sup>3</sup> Department of Geography, Presidency University, Kolkata, West Bengal, India

<sup>4</sup> Public Works Research Institute (PWRI), Tsukuba, Japan

<sup>5</sup> Cartography and Geographical Information System, School of Geographic Science, Nanjing, China

both the crop yield and soil fertility (Feinerman et al. 1982; Li et al. 2011, 2012; Elhag 2016). The global rise in mean sea level and the inundation of lowland areas have been the major drivers of saline water intrusion into proximate fertile arable lands. These drivers create far-reaching implications for coastal habitats (Schofield et al. 2001). Both primary and secondary processes of salinization are generally observed in coastal areas (Mashimbye 2013). Occurrence of floods, storm surges, and the inundation of low-lying tracts cause primary salinization while secondary salinization occurs due to excessive use of fertilizer use and improper land management practices (Wu et al. 2008). About 830 million ha of land constituting 7% of the earth's surface is vulnerable to salinization (FAO 2005, 2007; Abdelfattah et al. 2009).

Lack of accurate data is a major challenge for demarcating and analyzing salt-affected tracts in almost all the continents (Gupta and Abrol 1990; Rengasamy 2006). More pertinently, soil salinity is a great problem in various worldwide deltas (some of the most densely inhabited and intensively cultivated tracts) affecting not only the ambient vegetation conditions but also local livelihoods. For example, salinity intrusion in the lower Indus delta in Pakistan has severely affected agricultural activities and consequently displaced local residents (Giosan et al. 2014) while rising soil salinity along Bangladesh's south-west coast has impacted available ecosystem services. Inadequate monitoring measures have further resulted in degradation of the deltaic environment (Szabo et al. 2016). Improper land management practices and poor drainage condition arising from over irrigation have affected groundwater depth and salt concentration in the Nile delta (Mohamed et al. 2011). Increasing concentration of sulfate, sodium, and chloride ions have spurred on soil salinization in the Yellow River delta and China's eastern coast (Zhang et al. 2017).

In a similar vein, the coastal tracts of the Sundarban contain severely salt-affected soils and also face enhanced water salinity during the dry season each year (MoA and FAO 2013). Increasing concentration of soil salinity has markedly impaired agricultural activities therein. This area is prone to cyclones and storm surges (Chaudhuri and Choudhury 1994), with riverine and coastal erosion posing major threats to inhabited estuarine islands (Sahana et al. 2019; Sahana and Sajjad 2019). Several geo-physical and geo-hydrological factors such as tidal character, estuary and deltaic morphology, numerous tidal creeks, shallow offshore depths, convergence of the bay, and high astronomical tides cause disastrous storm surges (Mitra et al. 2009). As a result, large-scale variations in soil salinity are observed during the summer monsoon, pre-monsoon, and post-monsoon seasons (Mitra et al. 2009; Banerjee et al. 2013). Consequently, many agricultural fields are rendered fallow during the dry season, diminishing livelihoods and economic security. Such land degradation from enhanced salinity levels (whose future prospect seems even

more grim in a climate change scenario) potentially threatens the viability of the agricultural system of this deltaic area. Hence, identification and mapping of the salt-affected tracts in the area is essential for suggesting suitable management practices.

Conventional methods of soil salinity detection involving field surveys are expensive and time consuming. Geospatial technology has proved instrumental in monitoring spatiotemporal variations in salt-affected regions (Ben-Dor et al. 2009; Aldabaa et al. 2014). Multispectral remote-sensing data like Landsat, Terra-ASTER, IRS-LISS, SPOT series, MODIS (Dwivedi et al. 2008; Nawar et al. 2015), and hyperspectral data have been widely used for assessing soil salinity (Farifteh et al. 2007; Weng et al. 2008). Landsat TM and Landsat ETM+ datasets are preferably used for this purpose owing to their wide spectral band combination and enhancement quality (Sharma and Bhargava 1988; Wu et al. 2008). Image-extracted indices have also been analyzed through statistical measures like principal component analysis to predict soil salinity levels (Khan et al. 2001). However, the integration of satellite images and field datasets provides more accurate estimates of salinity levels (Bishop and McBratney 2001; Bouaziz et al. 2011). Many studies have established the relationship between measured soil electrical conductivity (EC) and satellite image-derived spectral indices, which can be then used to assess the soil quality (Garcia et al. 2005; Bouaziz et al. 2011). However, soil salinity assessment remained underemphasized in the Indian Sundarban Biosphere Reserve (SBR) using such approaches.

An attempt has thus been made in the present study to map the degree of soil salinity in SBR using spectral indices derived from Landsat-8 images, field-based measurements, and various statistical measures. For this, we have first provided a brief overview of the study area and outlined the various datasets used. We then explained the various field measurements and soil tests conducted and listed the indices extracted from the satellite data. The different datasets obtained thus were analyzed statistically to compare the laboratory results and image outputs. Suitable salinity indices were discerned based on the computed Pearson's correlation coefficient. These salinity indices were then integrated to map the salinity levels in the SBR. Finally, the relationships between the discerned soil salinity and different topographical variables were analyzed to gauge their respective degree of influence.

## Study area

The Sundarban Biosphere Reserve is located in the lower part of the Ganga-Brahmaputra-Meghna delta (Sharma et al. 2010). It spreads over 9630 km<sup>2</sup> and is demarcated by the Dampier-Hodges line to the north, the Bay of Bengal in the south, the Hooghly estuary in the west, and the Ichamati-

Raimangal River in the east. The Reserve covers south and north 24 Parganas districts of West Bengal located between 21° 31' N and 22° 30' N latitudes and 88° 10' E and 89° 51' E longitudes (Fig. 1).

Within the SBR, there are 48 uninhabited islands covering mangrove forests and 54 inhabited islands having settlement (Fig. 2). Most of the reserve consists of low-lying alluvial mud flats, tidal creeks, and multiple river channels. This deltaic region was formed in the Late Quaternary Period (2500 to 5000 years ago) as a result of long-term deposition of the sediments brought down by the *Ganga*, *Brahmaputra*, and *Meghna* rivers (Allison et al. 2003). Numerous creeks, estuaries, and rivers allow tidal inflow up to 300 km inland from the mouth of the *Ganga* along the Bay of Bengal (Sahana et al. 2015). The SBR can be divided into the core zone (1692 km<sup>2</sup>), buffer zone (2233 km<sup>2</sup>), and transition zone (5705 km<sup>2</sup>). The deltaic soil is mostly saline and consists of silt, clay, coarse sand, and fine sand particles. The National Bureau of Soil Survey & Land Use Planning (NBSS & LUP) has identified eleven distinct soil types in the SBR (Fig. 1; Table 1). The mainstay of the local economy is agriculture. However, the marked soil salinity levels herein often make this occupation uncertain and unsuitable (Sahana et al. 2016).

## Database and methods

An integrated approach was utilized, involving both field-based data of electrical conductivity and Landsat-8 OLI/

TIRS images for January 2018 to assess the soil salinity in the SBR. A total of 177 soil samples were collected from 59 locations during field survey conducted during January–February 2018, with at least one sample taken from within every 50 km<sup>2</sup> grid area inside the Sundarban Biosphere Reserve. A soil core of 1 m and 0–30 cm depth was taken from each sample site, and the locations of these sites were transferred onto the base map using coordinates recorded via a handheld GPS. The soil electrical conductivity (EC) provides a measure of the amount of salinity in the soil (Parsa et al. 2018) and is a crucial factor in determining its fertility, crop suitability, and water holding capacity (Barbosa and Overstreet 2011; USDA (United States Department of Agriculture), NRCS (National Resources Conservation Service) 2020). It further conditions the soil-water balance in the soil column and thereby affects the nature of plant growth within it (Ekeleme and Agunwamba 2018; Tint et al. 2018). The respective ECs of the collected samples were measured in the laboratory. The Tucker and Beatty (1974) method was used to determine the exchangeable bases (Ca<sup>2+</sup>, Mg<sup>2+</sup>, Na<sup>+</sup>, and K<sup>+</sup>) in the laboratory. The basic exchangeable cations were summed to compute the effective cation exchange capacity (ECEC). This is invariably equal to total cation exchange capacity (CEC), as the exchangeable acidity was negligible (Odeh and Onus 2008). Instrument calibration was done using potassium chloride (KCl) solution at 25 °C and was measured using 1:5 soil water suspension. Soluble salts in the soils were

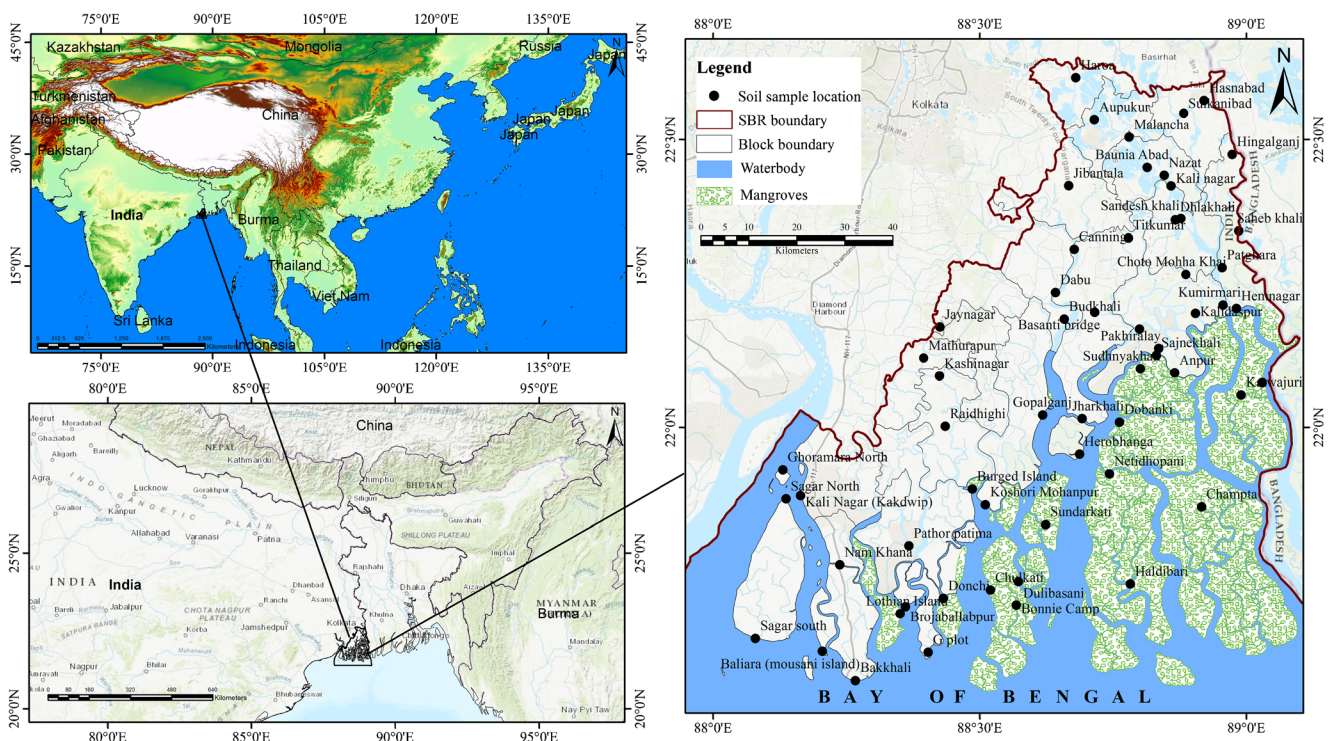
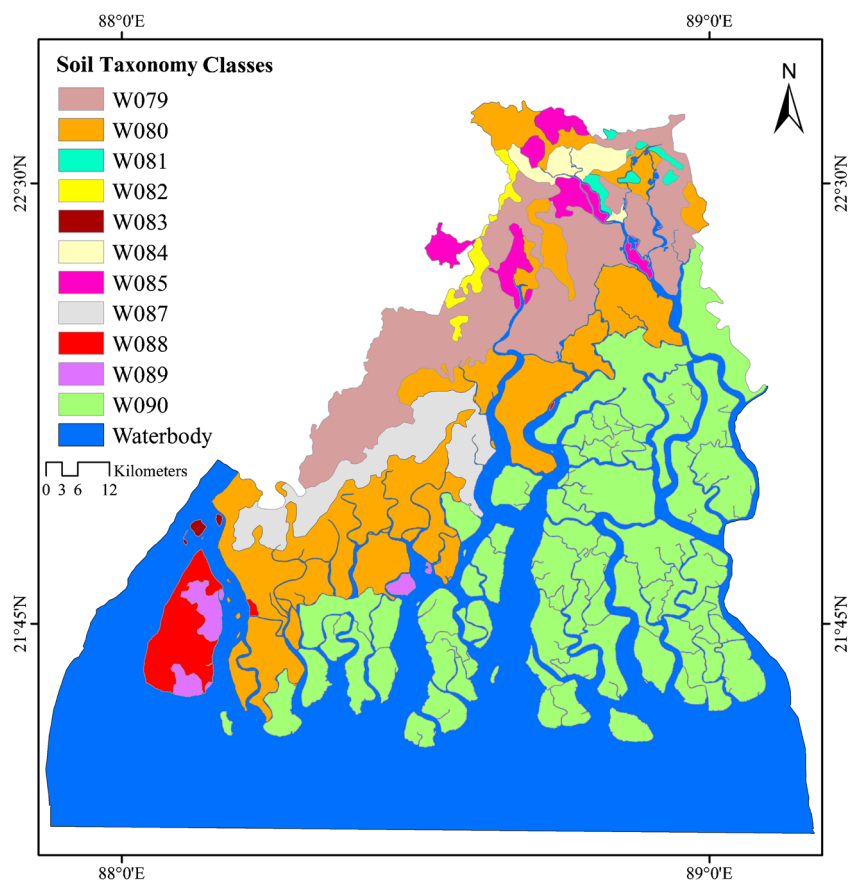


**Fig. 1** Location of the study area. **a** South Asia. **b** Location of SBR within eastern India. **c** Soil sample collection sites within the SBR

**Fig. 2** Soil classes in the Sundarban Biosphere Reserve (as identified by the NBSS and LUP)



determined by measuring the sodium, magnesium, calcium, and the anions  $\text{Cl}^-$ ,  $\text{SO}_4^{2-}$ , and  $\text{HCO}_3^-$  (Rayment and Higginson 1992). The solution was converted to saturated paste extract to estimate the EC. For calculating the EC, the Electrochemical Stability Index (ESI) was used (Eq. 1), following McKenzie (1998), as

$$\text{ESI} = \frac{\text{EC}}{\text{ESP}} \quad (1)$$

where, ESI = Electrochemical Stability Index, EC = electrical conductivity, and ESP = exchangeable sodium percentage.

The exchangeable sodium percentage (ESP) was estimated using Eq. 2 (after McKenzie 1998):

$$\text{ESP} = \frac{[\text{Na}^+]}{\text{ECEC}} \quad (2)$$

Various studies have used different satellite image-derived salinity indices for analyzing soil salinity (Bouaziz et al. 2011; Khan et al. 2001, 2005; Dehni and Lounis 2012). Based on the literature surveyed, we used eight prominent salinity indices and prepared their respective map outputs (Table 2). Subsequently, correlation analysis was performed between the values derived from these indices and the EC values

obtained from the field sample measurements for the corresponding points. The EC measured from the soil samples was found to be highly correlated with the satellite image-derived salinity index (SI-3) and the normalized difference salinity index (NDSI). The SI-3 parameter was computed by performing mathematical operations using the green, red, and near-infrared bands while the NDSI parameter was computed by normalizing the difference in the spectral reflectance of the red and near-infrared bands (Khan et al. 2005). NDSI parameter has been used in a number of soil salinity studies to assess the ambient salinization extent and severity (e.g., Elhag and Bahrawi 2016; Asfaw et al. 2018; Nguyen et al. 2020). Therefore, the SI-3 and the NSDI parameters' values were taken to best conform to the field-measured EC values.

The predicted EC values were obtained by assigning the pixel values of the NDSI and SI-3 outputs to the measured EC values. The relationship between the field-measured EC and this predicted EC was analyzed using corresponding pixels of the sampled locations, in which the measured EC value of a point was compared with the derived pixel value of that point. The final soil salinity layer derived from the above datasets was categorized into five classes based on its intensity, using the level slicing approach. The degree of salinity was determined based on the predicted EC values (2 dS/m, 4 dS/m, 8 dS/m, and 16 dS/m). Soil types (as per the soil taxonomy

**Table 1** Types of soil cover in the Sundarban Biosphere Reserve (nomenclature and classification as per soil taxonomy classification of the NBSS&LUP)

Soil code	Taxonomic name	Brief description
W079	Fine-loamy typic Haplaquepts Fine aeric Haplaquepts	Poorly drained, very deep, fine loamy occurring on leveled upper delta, sediments of many distributaries with loamy surface. Moderate salinity and severe flooding (limited extent)
W080	Fine typic Haplaquepts	Poorly drained, very deep, fine soil found in nearly level upper delta, sediments of many distributaries with loamy surface. Moderate salinity and severe flooding (limited extent)
W081	Fine aeric Haplaquepts, Fine-loamy typic Ustorthents	Poorly drained, very deep, fine soils occurring on upper delta to level surfaces plains, imperfectly drained, moderate flooding associated with very deep, fine loamy soils
W082	Fine-loamy aeric Haplaquents Fine-loamy aeric Haplaquepts	Poorly drained, very deep, fine loamy soils occurring on nearly level to level upper delta plain, poorly drained and subject to severe flooding, fine loamy soils
W083	Fine aeric Haplaquepts, Fine-loamy typic Haplaquepts	Poorly drained, very deep, fine loamy soils, fine soils occurring on nearly level to level upper delta plain with clayey surface, poorly drained soils subjected to severe flooding
W084	Fine aeric Haplaquepts, Fine typic Haplaquepts	Poorly drained, very deep, fine soils occurring on nearly level to level upper delta plain with clayey surface and subject to severe flooding, fine soils
W085	Fine aeric Haplaquepts, Fine typic Ustochrepts	Very deep soil, drained poorly, fine texture occurring on nearly level to level marshes, imperfectly drained and subject to severe flooding
W087	Fine aeric Haplaquepts, Fine typic Haplaquepts	Poorly drained, very deep, fine soils occurring on nearly level to level upper delta, inter distributary sediments with clayey surface, well drained sandy soils and thus moderate flooding
W088	Fine aeric Haplaquepts, Fine typic Haplaquepts	Poorly drained, very deep, fine soils occurring on nearly level to level lower delta having clayey surface with moderate salinity and severe flooding (moderate extent)
W089	Fine aeric Haplaquepts	Poorly drained, very deep, fine soils occurring on nearly level to level lower delta, clayey surface, moderate salinity and severe flooding
W090	Fine-loamy typic Haplaquepts, fine-loamy typic Fluvaquents	Poorly drained, very deep, fine soils occurring on nearly level to level lower delta, very strong salinity, severe flooding

Source: National Bureau of Soil Survey and Land Use Planning (NBSS&LUP)

classification obtained from the NBSS and LUP) were integrated with the predicted EC values to generalize the soil salinity map. The relationship between the EC (independent variable) and the salinity index (dependent variable) was

finally analyzed using linear and exponential regressions. Eight site-specific topography-related variables that are usually associated with soil salinity levels within the SBR were selected based on the literature survey and local field

**Table 2** Satellite data-derived salinity indices for preparing the soil salinity map of the SBR

	Equation	References
Salinity Index (SI)		
SI-1	$SI1 = \sqrt{\text{blue} \times \text{red}}$	Khan et al. (2005)
SI-2	$SI2 = \sqrt{\text{green} \times \text{red}}$	Khan et al. (2005)
SI-3	$SI3 = \sqrt{(\text{green})^2 + (\text{red})^2} + (\text{NIR})^2$	Douaoui et al. (2006)
SI-4	$SI4 = \sqrt{(\text{green})^2 + (\text{red})^2}$	Douaoui et al. (2006)
SI-5	$SI5 = \sqrt{\text{red} \times \text{NIR}}$	Dehni and Lounis (2012)
Brightness Index (BI)	$BI = \sqrt{(\text{red})^2 + (\text{NIR})^2}$	Khan et al. (2005)
Vegetation Soil Salinity Index (VSSI)	$VSSI = 2 \times \text{green} - 5 \times (\text{red} + \text{NIR})$	Dehni and Lounis (2012)
Normalized Difference Salinity Index (NDSI)	$NDSI = (\text{red} - \text{NIR}) + (\text{red} + \text{NIR})$	Khan et al. (2005)

knowledge. These variables included the local elevation, slope amount, surface plan curvature, stream power index (SPI), drainage density, and the distance from drainage lines. All these variables were transformed into raster grid spatial layers of  $30 \times 30$  m pixel size for creating a uniform thematic database (Fig. 3).

Shuttle radar topography mission (SRTM) digital elevation model (DEM) one arc-second data of 30 m spatial resolution (obtained from the United States Geological Survey repository) was used to assess the elevation, slope, surface curvature, and SPI values within the SBR. It offers worldwide coverage of void filled data. The surface altitude (both absolute and relative) assumes significance in soil salinity intrusion. Coastal lands are generally situated at quite low elevations, and thus are swamped easily during high tides and storm surges. These lands are further subject to the threat of submergence as sea levels rise. These conditions can increase the local soil salinity (Diez et al. 2007). There is also a direct relationship between this low elevation and the risk posed by natural hazards in coastal areas (Gornitz et al. 1994). The surface slope is an important physiographic

parameter that affects soil salinity in coastal regions. The study area was divided into three slope categories, such as less than  $2^\circ$ ,  $2^\circ$ , to  $5^\circ$  and greater than  $5^\circ$  (Fig. 4). About 75% of the study area falls within the  $0^\circ$ – $1^\circ$  slope class, and the overall slope ranged from  $0^\circ$  to  $6.3^\circ$ , and the entire region is mostly quite gently sloping. Negative and positive curvature values represent concave and convex surfaces, respectively, while zero curvature values denote flat surfaces (Fig. 4). A concave curvature surface has a greater effect on soil salinity in coastal regions than the convex surface, due to its abetting of water logging and surface erosion.

Drainage density is the ratio of the total drainage length within a cell area to the size of the respective cell area (Greenbaum 1989). Higher drainage density areas in coastal regions face a higher probability of salt-water intrusion into the top soil. The drainage network was digitized in the Google Earth platform and was converted to a raster layer in ArcGIS software. Five drainage density zones ( $0$ – $200$   $\text{m}/\text{km}^2$ ,  $200$ – $400$   $\text{m}/\text{km}^2$ ,  $400$ – $600$   $\text{m}/\text{km}^2$ ,  $600$ – $800$   $\text{m}/\text{km}^2$ , and more than  $800$   $\text{m}/\text{km}^2$ ) were demarcated within the study area (Fig. 4).

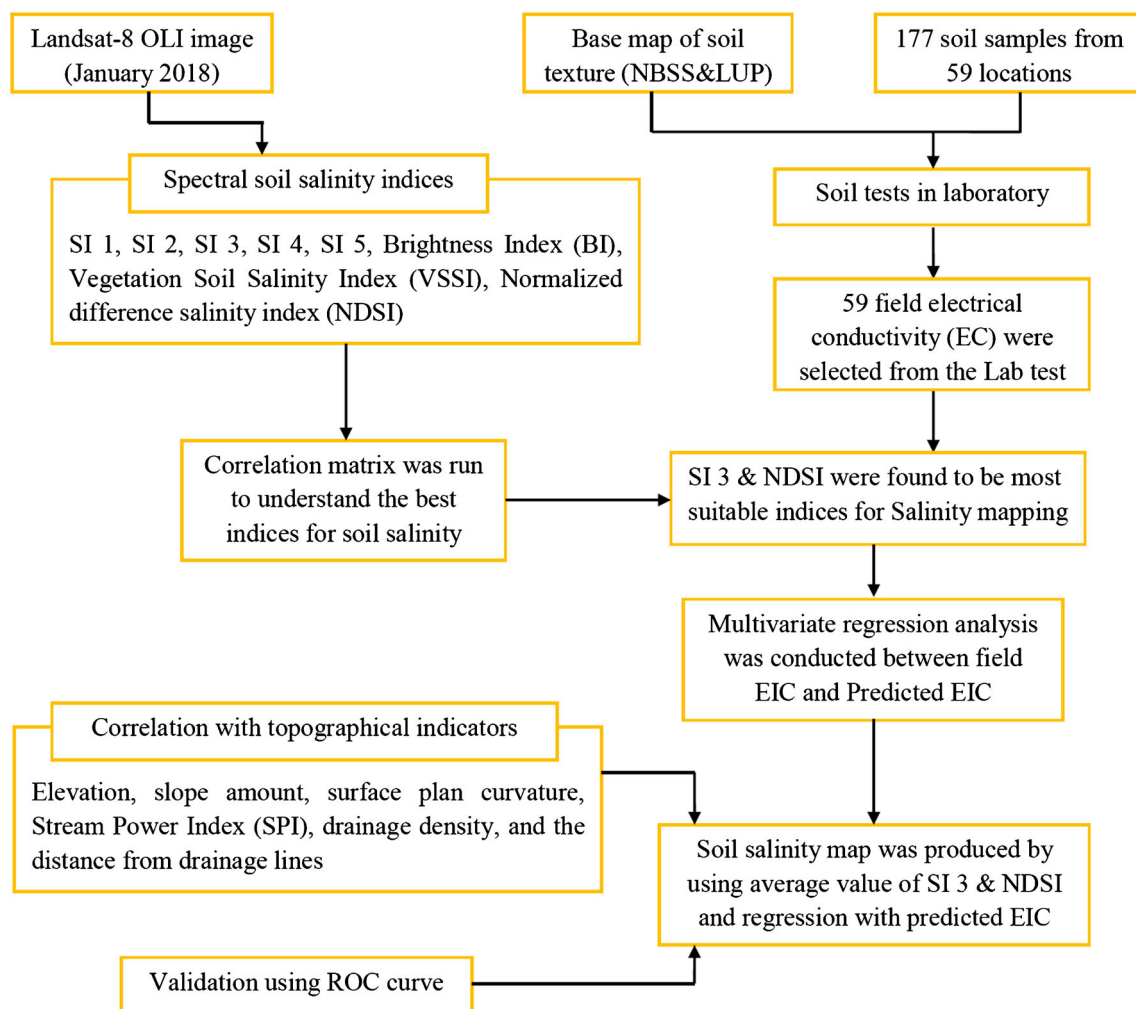
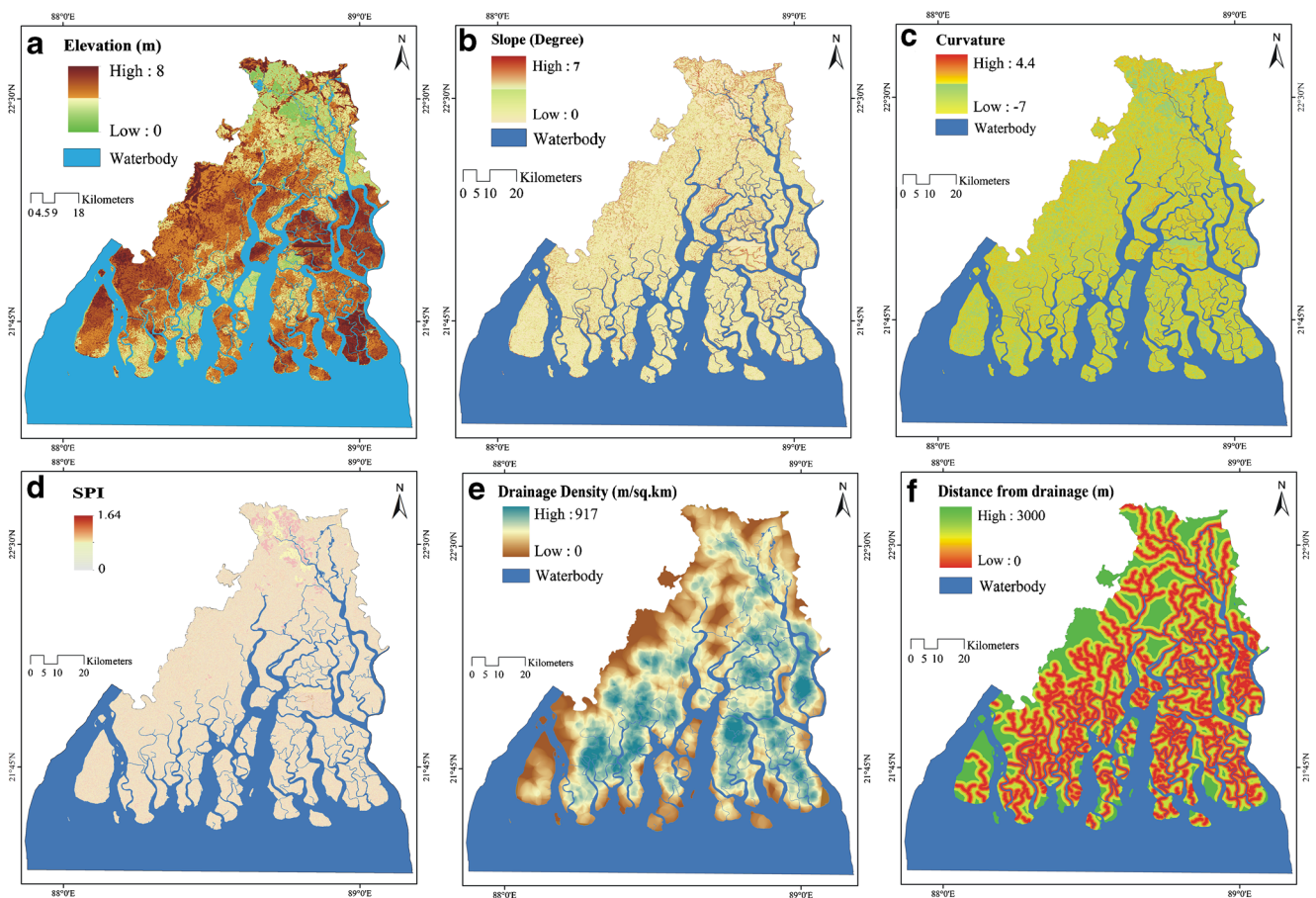


Fig. 3 Methodological framework adopted for assessing soil salinity in the SBR



**Fig. 4** Topographical indicators associated with soil salinity in the SBR. **a** Elevation (in m). **b** Slope (in degrees). **c** Curvature. **d** Stream power index. **e** Drainage density (in  $m/km^2$ ). **f** Distance from drainage lines (in m)

The stream power index (SPI) indicates the erosional power of streams (Moore et al. 1991) and is used for identifying those areas where surface runoff-induced erosion can be lessened through soil conservation measures (Tagil and Jenness 2008). It is calculated as (Eq. 3):

$$SPI = A_s \times \tan\beta \quad (3)$$

where  $A_s$  and  $\beta$  are the specific catchment area and the slope angle, respectively. The SPI was determined by running the D-8 flow accumulation and flow direction algorithms (cf. Patel and Sarkar 2010) on the SRTM DEM data (Figs. 4 and 5).

The distance of a particular site from the nearby river channels is one of the most important parameters influencing soil salinity in a coastal region. A distance to drainage map was generated from the SRTM DEM data using the hydrological tool in ArcGIS. Generally, places further located away from drainage lines experience less exposure to coastal/riverine flooding (Fig. 4).

Finally, the soil salinity map of the SBR was validated through the success and prediction rate curves under the receiving operating characteristics (ROC). The ROC curve

graphically displays the diagnostic capability of the performed analysis by comparing the true positive rate against the false positive rate and is thus widely used to ascertain the veracity of such computations (Bradley 1997; Hajian-Tilaki 2013). Various studies have assessed the overall accuracy of the enumerated field and predicted variables in this manner (e.g., Egan 1975; Sahana et al. 2018).

## Results and discussion

The amount of soil moisture, soil organic carbon content, the soil texture, and tone influences the spectral reflectance of the observed satellite data (Douaoui et al. 2006). Salt-affected soils in the SBR were assessed using the spectral reflectance derived from the utilized Landsat-8 images and from the sampled field data (Fig. 6). Eight soil spectral indices were initially extracted and from among them, the most apt ones (as determined through comparison with the field-measured EC values) were selected based on the ascertained correlation values (Table 3). The coefficient of determination ( $R^2$ ) was

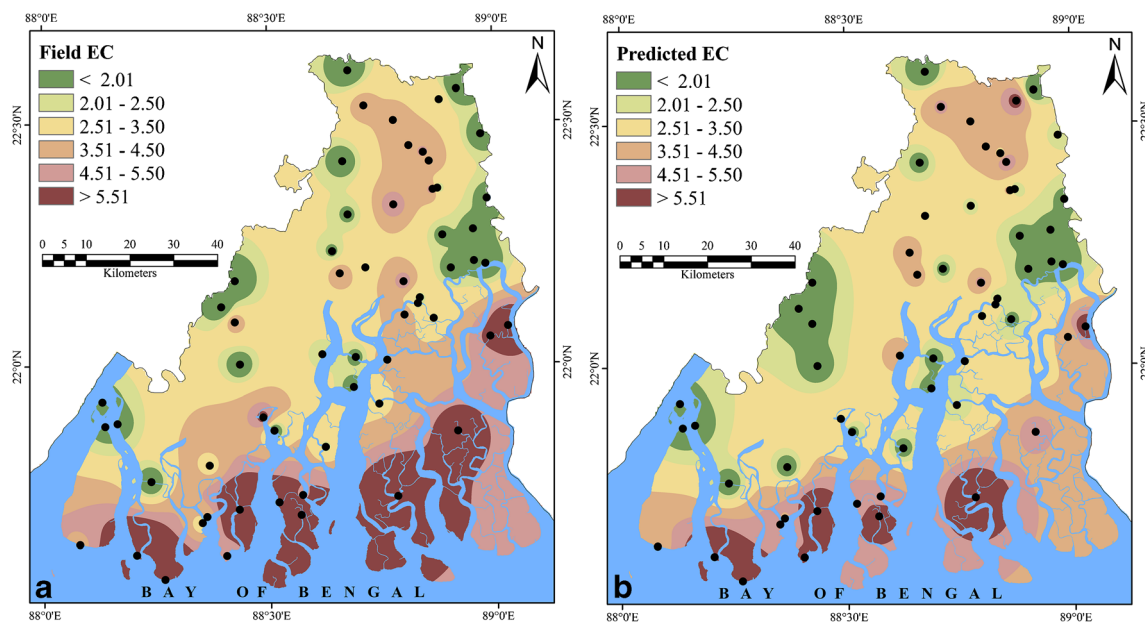


**Fig. 5** Electrical conductivity (EC) values in the SBR. **a** From field-measured soil samples. **b** The predicted EC values

highest in case of the Soil Salinity Index-3 (SI-3) ( $R^2 = 0.79$ ) and for the NDSI ( $R^2 = 0.76$ ). Hence, the SI-3 and the NDSI were determined as the best-fit indices for predicting the soil salinity in the study area. The correlations between the measured EC of the soil samples (Fig. 5a) and the values obtained through these two indices were found to be significant (with SI-3 less than 0.05 and NDSI less than 0.001). The predicted EC map was subsequently prepared using the averaged values of these two best-fit models and the field EC data (Fig. 5b).

Taking all the above cartographic products generated together, the final output, i.e., the soil salinity map of the SBR (Fig. 7), was eventually prepared by integrating the averaged values of the SI-3 and the NDSI (the two best-fit models) with the predicted EC values obtained above. The individual pixel values obtained in this final soil salinity map were grouped into five classes. These were extremely saline soil (EC greater than 8.0 dS/m), highly saline soil (EC between 6.1 dS/m and 8.0 dS/m), moderately saline soil (EC between 4.1 dS/m and 6.0 dS/m), slightly saline soil (EC between 2.1 dS/m and 4.0 dS/m), and very low/non-saline soil (EC less than 2.0 dS/m). The areal extents of each of these demarcated soil salinity zones were then determined, along with their respective mean EC values (Table 4).

The soil salinity map revealed that nearly 57% of the land in the SBR was affected to some extent by soil salinity (Table 4). Of the total area under saline soils, the largest area (18.8%) was under the highly saline soil followed by the slightly saline (17.2%), extremely saline (12.6%), and moderately saline (8.5%). Extremely saline soil is mostly found, as expected, along the coastal areas in mangrove forest patches and in lands proximate to the major waterways (Fig. 7). High salinity was found in places where prawn cultivation is a

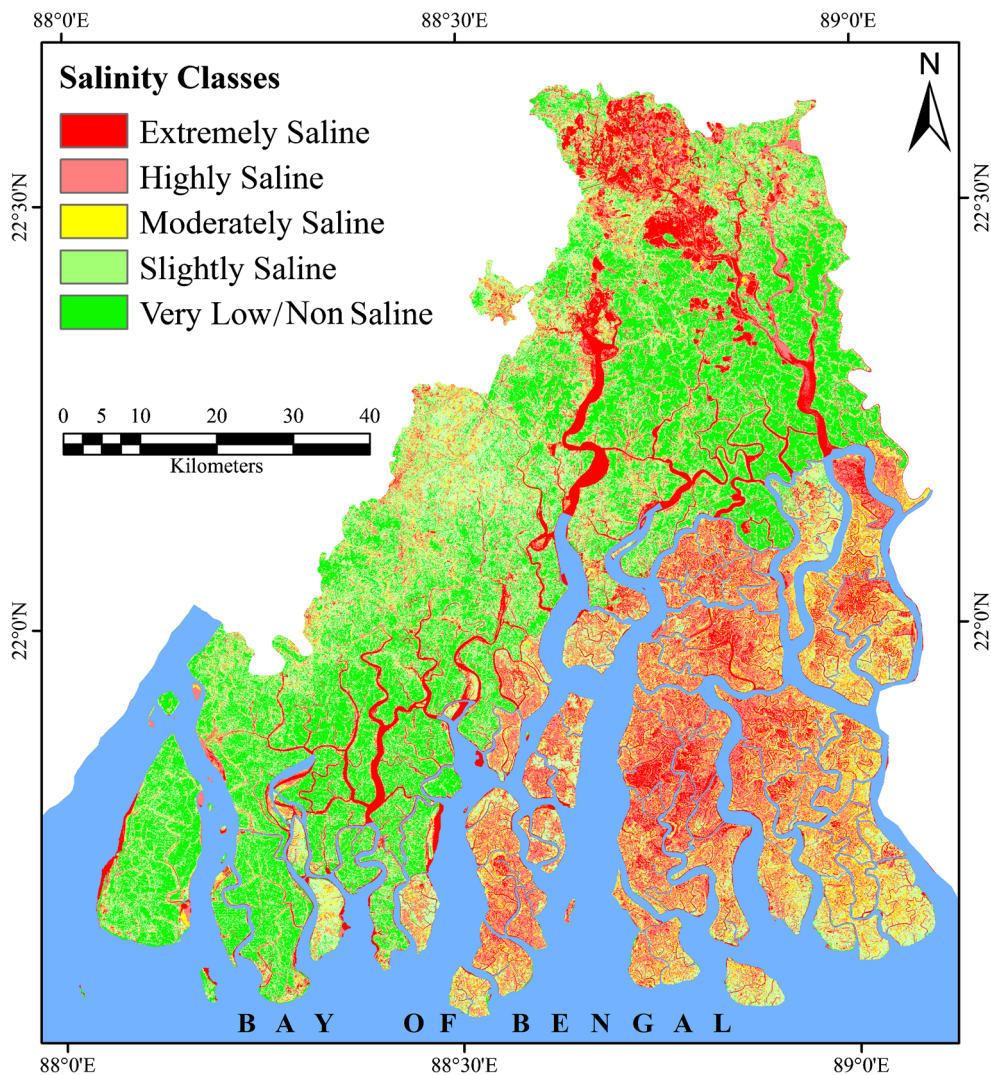
major economic activity. For this, water is collected and held within the various ponds during high tides, which eventually leads to water stagnation, evaporation, and the ensuing salt accumulation. Such areas are also located further inland from the coastline and alongside various rivers in the area. Highly saline soils were also found in the mangrove forests and swamps, mainly as a result of the daily tidal activity occurring in this estuarine region. Extremely saline soil was limited to lands bordering or situated near the main shoreline. Various coastal plantations are present on these very salty soils. In spite of the different measures undertaken to lessen the soil salinity (e.g., planting of trees that are tolerant to salinity), the ambient salinization has increased, engendering several negative impacts on the local agricultural sector, particularly in terms of diminishing crop productivity and soil fertility. Moderate salinity was mainly concentrated in the northern and northeastern part of the SBR and can be attributed to the high drainage density in this zone. Slightly saline and non-saline areas were located away from the coastline, and these tracts are being utilized for agriculture presently.

## Model validation

The soil salinity map was validated using the success rate curve and the prediction rate curve as per the ROC technique, which discerns the probability of a binary result (i.e., a correct or an incorrect prediction) in such analysis (Hand and Till 2001). Area under curve (AUC) is a measure of the model's performance and accuracy highlighting its degree of separability or ability to distinguish between different classes (Hand and Till 2001). In theory, AUC values can range from 0 to 1,



**Fig. 6** Soil salinity map prepared from the best-fit soil salinity model



with higher values nearer 1 indicating a robust and accurate model performance (Hosmer and Lemeshow 2000). The respective pixels of the different soil salinity classes were

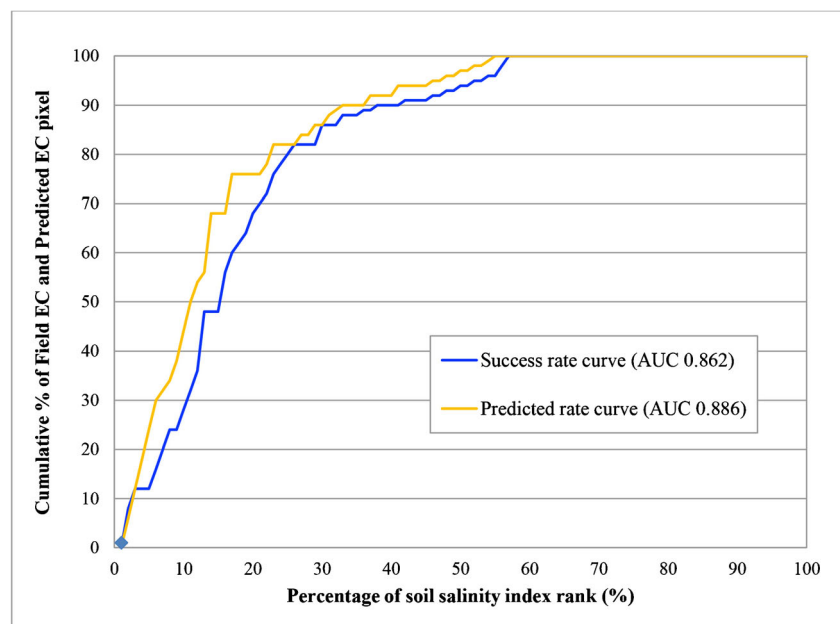
arranged in descending order to obtain their relative ranks. Thereafter, the values of the success rate curve and the prediction rate curve were determined as 0.862 and 0.886,

**Table 3** Correlation of electrical conductivity (EC) with salinity indices in the SBR

	$R^2$	Pearson correlation coefficient (r)
Salinity Index (SI)		
SI-1	0.58	0.36
SI-2	0.61	- 0.49**
SI-3	0.79	0.34*
SI-4	0.69	0.46
SI-5	0.71	0.33
Brightness Index (BI)	0.70	0.27
Vegetation Soil Salinity Index (VSSI)	0.68	- 0.25
Normalized difference salinity index (NDSI)	0.76	0.44**

Significance level \*\* $p < 0.001$ ; \*  $p < 0.05$

**Fig. 7** Receiver operating characteristics (ROCs) curve assessment for validating the soil salinity model



respectively. As the soil salinity model had high AUC values for both these curves (Fig. 8), the high accuracy and acceptability of the model devised was ascertained (e.g., Sahana and Patel 2019).

### Relationship between soil salinity and topography

The relationships between the demarcated salinity classes and various topographical variables (elevation, slope amount, surface plan curvature, SPI, drainage density, and the distance from drainage lines) were ascertained to discern which factors most influenced salinization in the study area (Plate 1). A negative linear relation was found between the soil salinity and surface elevation ( $R^2 = 0.624$ ), and therefore, the salinization intensities decreased with an increase in the altitude. Extreme soil salinity values (EC greater than 8) were generally found within a less than 2-m elevation from the coastline, with shallow and low-lying areas obviously being more frequently and extensively submerged, which increased their salinization levels. High and moderate soil salinity levels were found to be

generally concentrated within 2–6 m high surfaces. Very low/non-saline soils predominate on lands situated at greater than 6 m above the mean sea level. The surface slope and the soil salinity also have negative correlation ( $R^2 = 0.728$ ). The daily tidal activities are more prominent over the gently sloping land surfaces in the SBR, with incoming tidal bores washing across and inundating low-lying areas and increasing salinity levels therein. Both the extreme and highly saline zones mostly slope at less than  $1^\circ$ . Slightly steeper surfaces ( $4^\circ$ – $6^\circ$  slopes), in the northern part of the SBR, where the tidal bore effect would also be less pronounced, mostly have moderately saline to very low/non-saline soils.

The surface curvature also has a negative correlation with the soil salinity ( $R^2 = 0.825$ ). Areas with concave curvature (values less than 0) experience high to extreme soil salinity, due to the water logging effects while moderate to non-saline soils are found in convex curvature tracts. The SPI showed a positive correlation with the soil salinity ( $R^2 = 0.586$ ). High stream power enables more erosion and surface lowering and thereby increases the chances of salinization. Areas with SPI values greater than one showed high and extreme soil salinity levels. The drainage density also had a positive correlation with the soil salinity ( $R^2 = 0.614$ ), while it was negatively correlated with the distance to drainage line parameter ( $R^2 = 0.850$ ). Expectedly, areas along streams are likely to show higher salinization levels due to the tidal bores passing regularly through these channels, which bring in saline waters.

**Table 4** Areal extents of the different soil salinity classes discerned within the SBR

Value	EC value	Area in km <sup>2</sup>	Area in %
Extremely saline	> 8.0	1217	12.6
Highly saline	6.1 to 8	1807	18.8
Moderately saline	4.1 to 6.0	819	8.5
Slightly saline	2.1 to 4.0	1653	17.2
Very low/non saline	< 2.0	4136	42.9

### Distribution of soil salinity within the SBR

The derived soil salinity classes were overlain on a map of the SBR to analyze the proportion of the different salinity classes

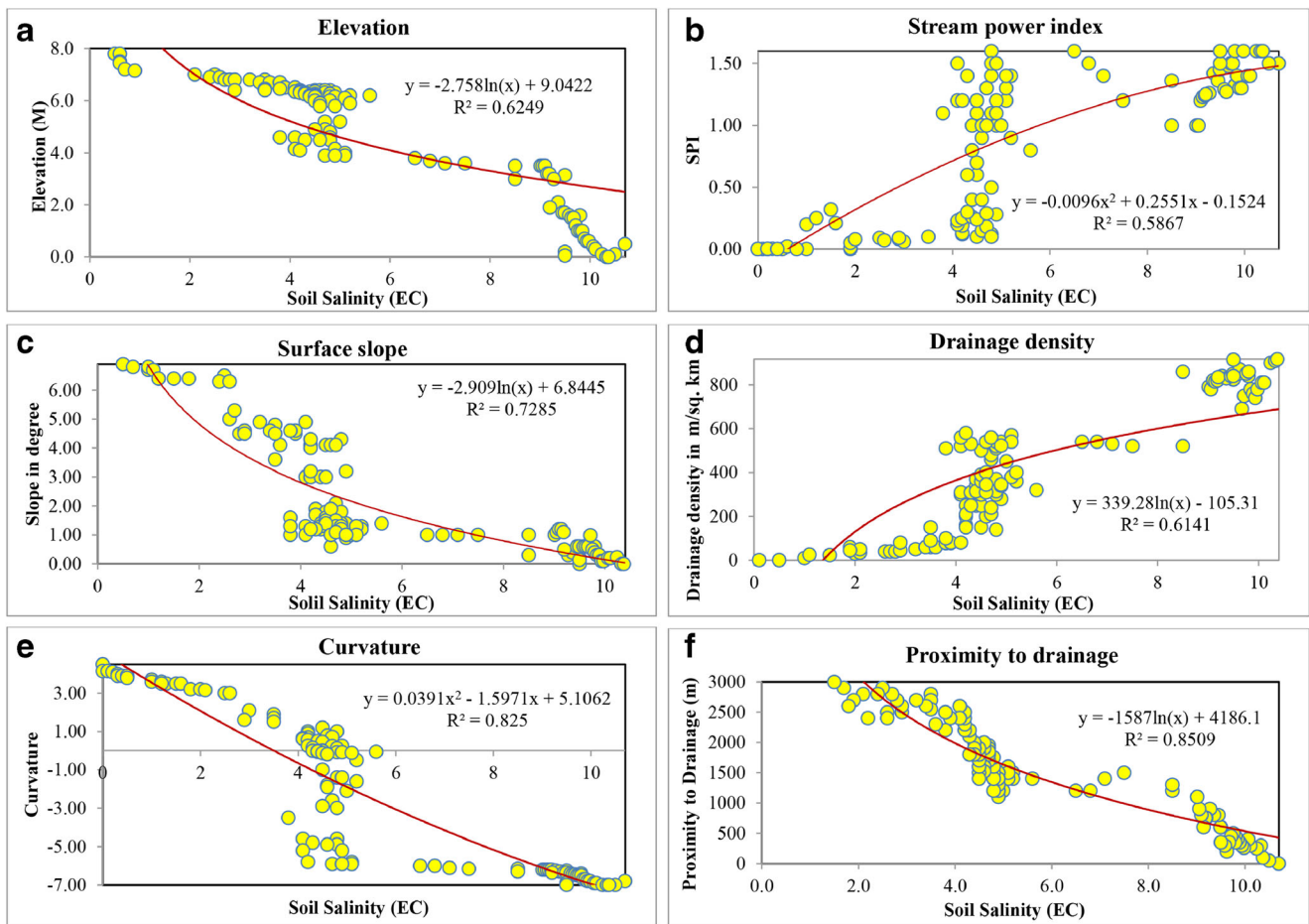
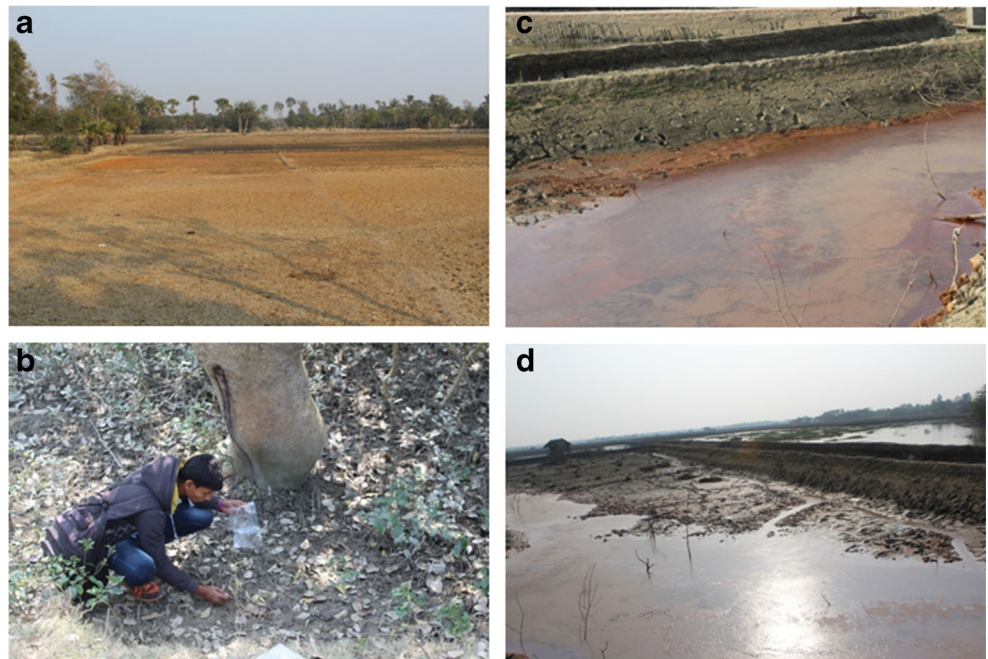


**Fig. 8** Relationships between the soil salinity and topographical characteristics of the study area. **a** Relation between soil salinity (EC) and elevation. **b** SPI and soil salinity (EC). **c** Surface slope and soil salinity (EC). **d** drainage density and soil salinity (EC). **e** Curvature and soil salinity (EC). **f** Proximity to drainage lines and soil salinity (EC)

**Plate 1** Photographs of the study area. **a** Salinity intrusion into agricultural land in Patharpratima block. **b** Soil samples collected for laboratory analysis. **c, d** Examples of salinity intrusion into the fish farms in Basanti block. Source: All field photographs were taken by the first author during surveys conducted in January 2018



present within each constituent block. While some tracts of extremely saline soils were concentrated in the northern part of the SBR (i.e., in Haroa Block), the maximum incursion and extent of the salt effect was seen along the southern part. In this zone, Patharpratima, Basanti, Kultali, Sagar, Sandeshkhali-I, and Gosaba blocks were all extremely affected by soil salinity due to their coastal and near-coastal locations. A greater proximity to drainage lines and high drainage density is responsible for the extreme soil salinity observed in the inland blocks of Haroa and Sandeshkhali-I (Table 5). High soil salinity stretched across parts of the Basanti, Minakhan, and Kultali coastal blocks. Frequent tidal inundation, gentle slopes, and the very low local elevation accounted for such high salt concentration in these places. Moderate soil salinity was observed in parts of Canning-II and Jaynagar-II blocks, in places that are situated relatively further away from the principal drainage lines. Most parts of Jaynagar-I, Canning-I, and Canning-II blocks have slightly saline soils owing to their further inland location and slightly higher surface elevation. The maximum concentration of very low/non-saline soils was observed in Mathurapur-I and Mathurapur-II blocks.

While the different soil salinity levels present in the various blocks could be deciphered quite accurately, this study does have some limitations arising from the relatively small number of soil sampling sites and the unevenness of the sampling site distribution over the study area. On average, only one sample could be collected from a 50-km<sup>2</sup> area, which reduces the accuracy levels of the study. The slight time difference between the image dataset used and the field surveys conducted can also produce some mismatches in the ascertained correlations. Furthermore, the use of a higher-resolution DEM for deriving the various topographic variables would elicit more accurate values (e.g., Das et al. 2016). Nevertheless, such an integration of field measurements and satellite image analysis has great potential in gauging salinity variations over a large region, with the method's simplicity and relative accuracy being its notable factors. Such monitoring of soil salinity along with similar assessments of the ambient surface water bodies and the local groundwater table is essential for deciphering the extent of this hazard in the region.

**Table 5** Degree of salinity ascertained in the different administrative blocks of the SBR with their respective areal coverage

Sl. No.	Community Development Blocks	Salinity Classes									
		Extremely saline		Highly saline		Moderately saline		Slightly saline		Very low/non saline	
		Area (sq.km)	Area (%)	Area (sq.km)	Area (%)	Area (sq.km)	Area (%)	Area (sq.km)	Area (%)	Area (sq.km)	Area (%)
1	Mathurapur-I	2.9	0.2	17.7	1.0	18.3	2.2	117.0	7.1	357.2	8.6
2	Jaynagar-I	5.8	0.5	26.1	1.4	24.3	3.0	170.0	10.3	44.3	1.1
3	Jaynagar-II	6.6	0.5	19.3	1.1	20.1	2.4	82.0	5.0	116.2	2.8
4	Kakdwip	12.4	1.0	24.3	1.3	20.2	2.5	75.4	4.6	275.6	6.7
5	Sagar	14.8	1.2	25.8	1.4	16.8	2.0	66.0	4.0	305.8	7.4
6	Hasnabad	17.6	1.4	50.2	2.8	23.4	2.9	59.9	3.6	199.9	4.8
7	Namkhana	19.5	1.6	26.3	1.5	17.2	2.1	59.6	3.6	114.7	2.8
8	Hingalganj	20.7	1.7	25.1	1.4	12.0	1.5	36.8	2.2	261.9	6.3
9	Mathurapur-II	30.4	2.5	27.6	1.5	21.9	2.7	78.8	4.8	321.3	7.8
10	Canning-II	37.6	3.1	39.2	2.2	24.8	3.0	170.3	10.3	278.9	6.7
11	Sandeshkhali-II	40.9	3.4	38.1	2.1	10.9	1.3	31.9	1.9	325.1	7.9
12	Canning-I	45.0	3.7	30.8	1.7	19.1	2.3	110.2	6.7	353.6	8.5
13	Kultali	46.8	3.8	56.5	3.1	30.5	3.7	112.9	6.8	217.0	5.2
14	Haroa	54.1	4.4	43.8	2.4	14.1	1.7	32.3	2.0	47.6	1.2
15	Minakhan	59.8	4.9	73.6	4.1	23.4	2.9	34.5	2.1	35.5	0.9
16	Gosaba	65.4	5.4	33.5	1.9	21.9	2.7	71.1	4.3	315.0	7.6
17	Sandeshkhali-I	68.5	5.6	43.7	2.4	13.4	1.6	32.4	2.0	116.8	2.8
18	Basanti	69.1	5.7	76.4	4.2	42.9	5.2	64.7	3.9	254.7	6.2
19	Patharpratima	79.9	6.6	43.0	2.4	29.3	3.6	67.5	4.1	157.3	3.8
20	Uninhabited area	520.3	42.7	1086.6	60.1	415.3	50.7	180.5	10.9	39.1	0.9

The % areal coverage has been done to show the proportionate coverage of each salinity class within the respective blocks

## Conclusion

Soil salinization is an ongoing environmental problem in the Sundarbans. The present study has analyzed the soil salinity in the Indian part of the SBR using multispectral Landsat-8 images along with field-sampled and laboratory-measured soil samples. The EC values obtained from a total of 177 soil samples collected across the study area were used to determine the most suitable soil salinity indices extracted from the image datasets. Soil salinity classes were obtained by combining these indices with the field-measured and predicted EC values, which were then validated through the ROC curve. The soil salinity map finally prepared revealed high and extremely high soil salinity levels to exist in the coastal deltaic islands, with these two classes respectively covering 12.6% and 18.8% of the SBR's total area. The blocks of Patharpratima, Basanti, Sandeshkhali-I, Gosaba, and Haroa were found to be most affected by the incidence of such enhanced soil salinity levels in the SBR. Relatively lower salinity levels were noted in Minakhan and Kultali blocks. If such salinization persists and becomes more widespread, it can engender marked ecological implications and pose further challenges to the largely subsistence of agriculture-based livelihoods in the study area. Revitalization of the local halophytic vegetation cover, minimizing water stagnation, and improving drainage conditions can provide some succor toward addressing this issue. The lining of the riverbanks in this region by the indigenous vetiver grass can help abate erosion (Mondal and Patel 2020) and decrease flood peaks (Mondal and Patel 2018), which would restrict the incursion of saline waters further inland and also allow absorption to some extent of the present salts and other pollutants in the water (Cuong et al. 2015; Liu et al. 2016), thereby reducing the salinity to a certain degree. The utilized integrated approach in this study that combined field, laboratory, and satellite data-based analysis was proven to be effective in estimating and mapping the ambient soil salinity levels quite accurately. Thus, this method can be feasibly employed in similar low-lying coastal and estuarine areas for assessing the existing degree of soil salinity therein at various spatial scales and for subsequently suggesting suitable management strategies.

**Acknowledgments** The authors would like to thank all the anonymous reviewers and Prof. Stefan Grab for their insightful comments and valuable suggestions, which helped us to improve the over the overall quality of the manuscript. We are grateful to Suvon Roy, Aziz Sahana, Nuhul Hussain and Devjeet Chatterjee for their help during the fieldwork. We are also thankful to the respondents of the villages of the Sundarban Biosphere Reserve in India for being so generous with their valuable time and opinions during the field survey.

## References

- Abdelfattah MA, Shahid SA, Othman YR (2009) Soil salinity mapping model developed using RS and GIS: a case study from Abu Dhabi, United Arab Emirates. *Eur J Sci Res* 26(3):342–351 <http://www.eurojournals.com/ejsr.htm>
- Aldabaa AAA, Weindorf DC, Chakraborty S, Sharma A, Li B (2014) Combination of proximal and remote sensing methods for rapid soil salinity quantification. *Geoderma* 239–240:34–46. <https://doi.org/10.1016/j.geoderma.2014.09.011>
- Allison MA, Khan SR, Goodbred SL Jr, Kuehl SA (2003) Stratigraphic evolution of the late Holocene Ganges-Brahmaputra lower delta plain. *Sediment Geol* 155(3–4):317–342. [https://doi.org/10.1016/S0037-0738\(02\)00185-9](https://doi.org/10.1016/S0037-0738(02)00185-9)
- Asfaw E, Suryabhagavan KV, Argaw M (2018) Soil salinity modeling and mapping using remote sensing and GIS: the case of Wonji sugar cane irrigation farm, Ethiopia. *J Saudi Soc Agric Sci* 17(3):250–258. <https://doi.org/10.1016/j.jssas.2016.05.003>
- Banerjee K, Sengupta K, Raha A, Mitra A (2013) Salinity based allometric equations for biomass estimation of Sundarban mangroves. *Biomass Bioenergy* 56:382–391. <https://doi.org/10.1016/j.biombioe.2013.05.010>
- Barbosa RN, Overstreet C (2011) What is soil electrical conductivity? LSU AgCenter (Louisiana State University Agricultural Center) Pub 3185. Available at <https://www.lsuagcenter.com/Nr/Rdonlyres/E57e82a0-3b99-4de9-99b5cf2ad7c43aef/77101/Pub3185whatissoilelectricalconductivityhighres.Pdf> Accessed 30 Sept 2020
- Ben-Dor E, Chabrillat S, Dematté JAM, Taylor GR, Hill J, Whiting ML, Sommer S (2009) Using imaging spectroscopy to study soil properties. *Remote Sens Environ* 113:S38–S55. <https://doi.org/10.1016/j.rse.2008.09.019>
- Bishop TFA, McBratney AB (2001) A comparison of prediction method for the creation of field-extent soil property maps. *Geoderma* 103: 149–160. [https://doi.org/10.1016/S0016-7061\(01\)00074-X](https://doi.org/10.1016/S0016-7061(01)00074-X)
- Bouaziz M, Matschullat J, Gloaguen R (2011) Improved remote sensing detection of soil salinity from a semi-arid climate in Northeast Brazil. *Compt Rendus Geosci* 343:795–803. <https://doi.org/10.1016/j.crte.2011.09.003>
- Bradley AP (1997) The use of the area under the ROC curve in the evaluation of machine learning algorithms. *Pattern Recogn* 30(7): 1145–1159. [https://doi.org/10.1016/S0031-3203\(96\)00142-2](https://doi.org/10.1016/S0031-3203(96)00142-2)
- Chaudhuri AB, Choudhury A (1994) Mangroves of the Sundarbans. Volume 1: India. International Union for Conservation of Nature and Natural Resources (IUCN)
- Cuong DC, Van Minh V, Troung P (2015) Effects of sea water salinity on the growth of Vetiver Grass (*Chrysopogon Zizanioides L.*). *Modern Environ Sci Eng* 1(4):185–191. [https://doi.org/10.15341/mese\(2333-2581\)/04.01.2015/004](https://doi.org/10.15341/mese(2333-2581)/04.01.2015/004)
- Daliakopoulos IN, Tsanis IK, Koutroulis A, Kourgialas NN, Varouchakis AE, Karatzas GP, Ritsema CJ (2016) The threat of soil salinity: a European scale review. *Sci Total Environ* 573:727–739. <https://doi.org/10.1016/j.scitotenv.2016.08.177>
- Das S, Patel PP, Sengupta S (2016) Evaluation of different digital elevation models for analyzing drainage morphometric parameters in a mountainous terrain: a case study of the Supin–Upper Tons Basin, Indian Himalayas. *SpringerPlus* 5:1544. <https://doi.org/10.1186/s40064-016-3207-0>
- Dehni A, Lounis M (2012) Remote sensing techniques for salt affected soil mapping: application to the Oran region of Algeria. *Procedia Eng* 33:188–198. <https://doi.org/10.1016/j.proeng.2012.01.1193>
- Diez PG, Perillo GM, Piccolo MC (2007) Vulnerability to sea-level rise on the coast of the Buenos Aires Province. *J Coast Res* 119–126. <https://doi.org/10.1007/s12517-017-3062-5>

- Douaoui AEK, Nicolas H, Walter C (2006) Detecting salinity hazards within a semi-arid context by means of combining soil and remote-sensing data. *Geoderma* 134(1-2):217–230. <https://doi.org/10.1016/j.geoderma.2005.10.009>
- Dwivedi RS, Kothapalli RV, Singh AN, Metternicht G, Zinck J (2008) Generation of farm level information on salt-affected soils using IKONOS-II multispectral data. In: Metternicht G, Zinck J (eds) *Remote Sensing of Soil Salinization: Impact on Land Management*. CRC Press, Taylor & Francis, Boca Raton, pp 73–90
- Egan JP (1975) *Signal detection theory and ROC analysis*. Academic Press, New York
- Ekeleme AC, Agunwamba JC (2018) Experimental determination of dispersion coefficient in soil. *Emerg Sci J* 2(4):213–218. <https://doi.org/10.28991/esj-2018-01145>
- Elhag M (2016) Evaluation of different soil salinity mapping using remote sensing techniques in arid ecosystems, Saudi Arabia. *J Sensors* 2016:7596175. <https://doi.org/10.1155/2016/7596175>
- Elhag M, Bahrawi JA (2016) Soil salinity mapping and hydrological drought indices assessment in arid environments based on remote sensing techniques. *Geosci Instrum Method Data Syst Discuss*. <https://doi.org/10.5194/gi-2016-39>
- FAO (2005) *Management of irrigation-induced salt affected soils*. Rome (Italy). CISEAU/FAO/IPTRID. [ftp://ftp.fao.org/agl/agll/docs/salinity\\_brochure\\_eng.pdf](ftp://ftp.fao.org/agl/agll/docs/salinity_brochure_eng.pdf) Accessed 15 Sept 2018.
- FAO (2007) *Extent and causes of salt-affected soils in participating countries*. AGL: Global network on integrated soil management for sustainable use of salt-affected soils, <http://www.fao.org/ag/agll/spush/topic2.html> Accessed 15 Sept 2018.
- Farifteh J, Van der Meer FD, Atzberger C, Carranza EJM (2007) Quantitative analysis of salt-affected soil reflectance spectra: a comparison of two adaptive methods (PLSR and ANN). *Remote Sens Environ* 110(1):5978–5978. <https://doi.org/10.1016/j.rse.2007.02.005>
- Feinerman E, Yaron D, Bielora H (1982) Linear crop response functions to soil salinity with a threshold salinity level. *Water Resour Res* 18(1):101–106. <https://doi.org/10.1029/WR018i001p00101>
- Garcia L, Eldeiry A, Elhaddad A (2005) Estimating soil salinity using remote sensing data. Proceedings of the 2005 Central Plains Irrigation Conference, 1-10. Available at <https://www.kstre.k-state.edu/irrigate/oow/p05/Garcia.pdf> Accessed 30 Sept 2020.
- Giosan L, Syvitski J, Constantinescu S, Day J (2014) Climate change: protect the world's deltas. *Nat News* 516(7529):31–33. <https://doi.org/10.1038/516031a>
- Gornitz VM, Daniels RC, White TW, Birdwell KR (1994) The development of a coastal risk assessment database: vulnerability to sea-level rise in the US Southeast. *J Coast Res*:327–338
- Greenbaum D (1989) Hydrogeological applications of remote sensing in areas of crystalline basement. In: *Proc Groundwater Exploration and Development in Crystalline Basement Aquifers, Zimbabwe*
- Gupta RK, Abrol IP (1990) Salt-affected soils: their reclamation and management for crop production. *Adv Soil Sci* 11:223–288. [https://doi.org/10.1007/978-1-4612-3322-0\\_7](https://doi.org/10.1007/978-1-4612-3322-0_7)
- Hajian-Tilaki K (2013) Receiver Operating Characteristic (ROC) Curve analysis for medical diagnostic test evaluation. *Caspian J Intern Med* 4(2):627–635
- Hand DJ, Till RJ (2001) A simple generalisation of the area under the ROC curve for multiple class classification problems. *Mach Learn* 45:171–186. <https://doi.org/10.1023/A:1010920819831.pdf>
- Hosmer DW, Lemeshow S (2000) *Applied logistic regression*. Wiley, Me York
- Jingwei W, Vincent B, Yang J, Bouarfa S, Vidal A (2008) Remote sensing monitoring of changes in soil salinity: a case study in Inner Mongolia, China. *Sensors* 8:7035–7049. <https://doi.org/10.3390/s8117035>
- Khan NM, Rastoskuev VV, Shalina E, Sato Y (2001) Mapping salt affected soil using remote sensing indicators. A simple approach with the use of GisIdrissi. 22nd Asian Conference on Remote Sensing, 5-9 November, Singapore
- Khan NM, Rastoskuev VV, Sato Y, Shiozawa S (2005) Assessment of hydrosaline land degradation by using a simple approach of remote sensing indicators. *Agric Water Manag* 77(1-3):96–109. <https://doi.org/10.1016/j.agwat.2004.09.038>
- Li DJ, Chun WM, Tiyyip T (2011) Study on soil salinization information in arid region using remote sensing technique. *Agric Sci China* 10(3):404–411
- Li J, Pu L, Zhu M, Zhang R (2012) The present situation and hot issues in the salt-affected soil research. *Acta Geograph Sin* 67:1233–1245. <https://doi.org/10.11821/xb201209008>
- Liu W, Liu J, Yao M, Ma Q (2016) Salt tolerance of a wild ecotype of vetiver grass (*Vetiveria zizanioides* L.) in southern China. *Bot Stud* 57:27. <https://doi.org/10.1186/s40529-016-0142-x>
- Mashimbye PM (2013) *Spherulites as evidence for herding strategies in the Mapungubwe cultural landscape*. Unpublished MSc Thesis, University of the Witwatersrand, Johannesburg. Available at <http://wiredspace.wits.ac.za/bitstream/handle/10539/12907/PM%20Mashimbye.pdf> Accessed 30 Sept 2020
- McKenzie DC (1998) *SOILpak for cotton growers*, 3rd edn. NSW Agriculture, Orange
- Mitra A, Gangopadhyay A, Dube A, Schmidt AC, Banerjee K (2009) Observed changes in water mass properties in the Indian Sundarbans (northwestern Bay of Bengal) during 1980-2007. *Curr Sci*:1445–1452
- MoA and FAO (2013) *Master plan for agricultural development in the southern region of Bangladesh*. Ministry of Agriculture, GoB. Available at <http://www.fao.org/3/a-au752e.pdf> Accessed 30 Sept 2020
- Mohamed ES, Morgun EG, Bothina SG (2011) Assessment of soil salinity in the Eastern Nile Delta (Egypt) using geoinformation techniques. *Moscow Univ Soil Sci Bull* 66(1):11–14. <https://doi.org/10.3103/S0147687411010030>
- Mondal S, Patel PP (2018) Examining the utility of river restoration approaches for flood mitigation and channel stability enhancement: a recent review. *Environ Earth Sci* 77:195. <https://doi.org/10.1007/s12665-018-7381-y>
- Mondal S, Patel PP (2020) Implementing Vetiver grass-based riverbank protection programmes in rural West Bengal, India. *Nat Hazards* 103:1051–1076. <https://doi.org/10.1007/s11069-020-04025-5>
- Moore ID, Grayson RB, Ladson AR (1991) Digital terrain modelling: a review of hydrological, geomorphological, and biological applications. *Hydrol Process* 5(1):3–30. <https://doi.org/10.1002/hyp.3360050103>
- Nawar S, Buddenbaum H, Hill J (2015) Digital mapping of soil properties using multivariate statistical analysis and ASTER data in an arid region. *Remote Sens* 7(2):1181–1205. <https://doi.org/10.3390/rs70201181>
- Nguyen K, Liou Y, Tran H, Hoang P, Nguyen T (2020) Soil salinity assessment by using near-infrared channel and Vegetation Soil Salinity Index derived from Landsat 8 OLI data: a case study in the Tra Vinh Province, Mekong Delta, Vietnam. *Prog Earth Planet Sci* 7:1. <https://doi.org/10.1186/s40645-019-0311-0>
- Odeh IO, Onus A (2008) Spatial analysis of soil salinity and soil structural stability in a semiarid region of New South Wales, Australia. *Environ Manag* 42(2):265–278
- Parsa N, Khajouei G, Masigol M, Hasheminejad H, Moheb A (2018) Application of electrodialysis process for reduction of electrical conductivity and COD of water contaminated by composting leachate. *Civil Eng J* 4(5):1034–1045. <https://doi.org/10.28991/cej-0309154>
- Patel PP, Sarkar A (2010) Terrain characterization using SRTM data. *J Indian Soc Remote Sens* 38:11–24. <https://doi.org/10.1007/s12524-010-0008-8>
- Rayment GE, Higginson FR (1992) *Australian laboratory handbook of soil and water chemical methods*. Inkata Press, Melbourne

- Rengasamy P (2006) World salinization with emphasis on Australia. *J Exp Bot* 57(5):1017–1023. <https://doi.org/10.1093/jxb/erj108>
- Sahana M, Patel PP (2019) A comparison of frequency ratio and fuzzy logic models for flood susceptibility assessment of the lower Kosi River Basin in India. *Environ Earth Sci* 78:289. <https://doi.org/10.1007/s12665-019-8285-1>
- Sahana M, Sajjad H (2019) Assessing influence of erosion and accretion on landscape diversity in Sundarban Biosphere Reserve, lower Ganga basin: a geospatial approach. In: Das BC, Ghosh S, Islam A (eds) *Quaternary Geomorphology in India*. Springer, Cham, pp 191–203. [https://doi.org/10.1007/978-3-319-90427-6\\_10](https://doi.org/10.1007/978-3-319-90427-6_10)
- Sahana M, Sajjad H, Ahmed R (2015) Assessing spatio-temporal health of forest cover using forest canopy density model and forest fragmentation approach in Sundarban reserve forest, India. *Model Earth Syst Environ* 1(4):49. <https://doi.org/10.1007/s40808-015-0043-0>
- Sahana M, Ahmed R, Sajjad H (2016) Analyzing land surface temperature distribution in response to land use/land cover change using split window algorithm and spectral radiance model in Sundarban Biosphere Reserve, India. *Model Earth Syst Environ* 2(2):81. <https://doi.org/10.1007/s40808-016-0135-5>
- Sahana M, Hong H, Sajjad H, Liu J, Zhu AX (2018) Assessing deforestation susceptibility to forest ecosystem in Rudraprayag district, India using fragmentation approach and frequency ratio model. *Sci Total Environ* 627:1264–1275. <https://doi.org/10.1016/j.scitotenv.2018.01.290>
- Sahana M, Hong H, Ahmed R, Patel PP, Bhakat P, Sajjad H (2019) Assessing coastal island vulnerability in the Sundarban Biosphere Reserve, India, using geospatial technology. *Environ Earth Sci* 78:304. <https://doi.org/10.1007/s12665-019-8293-1>
- Schofield R, Thomas D, Kirkby MJ (2001) Causal processes of soil salinization in Tunisia, Spain and Hungary. *Land Degrad Dev* 12(2):163–181. <https://doi.org/10.1002/ldr.446>
- Sharma RC, Bhargava GP (1988) Landsat imagery for mapping saline soils and wet lands in north-west India. *J Remote Sens* 9(1):39–44. <https://doi.org/10.1080/01431168808954835>
- Sharma RK, Jhala Y, Qureshi Q, Vattakaven J, Gopal R, Nayak K (2010) Evaluating capture-recapture population and density estimation of tigers in a population with known parameters. *Anim Conserv* 13(1):94–103. <https://doi.org/10.1111/j.1469-1795.2009.00305.x>
- Shrestha RP (2006) Relating soil electrical conductivity to remote sensing and other soil properties for assessing soil salinity in northeast Thailand. *Land Degrad Dev* 17:677–689. <https://doi.org/10.1002/ldr.752>
- Szabo S, Hossain MS, Adger WN, Matthews Z, Ahmed S, Lázár AN, Ahmad S (2016) Soil salinity, household wealth and food insecurity in tropical deltas: evidence from south-west coast of Bangladesh. *Sustain Sci* 11(3):411–421. <https://doi.org/10.1007/s11625-015-0337-1>
- Tagil S, Jenness J (2008) GIS-based automated landform classification and topographic, landcover and geologic attributes of landforms around the Yazoren Polje, Turkey. *J Appl Sci* 8(6):910–921. <https://doi.org/10.3923/jas.2008.910.921>
- Tint ZL, Kyaw NM, Kyaw K (2018) Development of soil distribution and liquefaction potential maps for downtown area in Yangon, Myanmar. *Civil Eng J* 4(3):689–701. <https://doi.org/10.28991/cej-0309108>
- Tucker BM, & Beatty HJ (1974) Exchangeable cations and cation exchange capacity. *Methods for analysis of irrigated soils*. (Ed. J Loveday) Technical Communication, (54)
- USDA (United States Department of Agriculture), NRCS (National Resources Conservation Service) (2020) Soil electrical conductivity. Soil Quality Kit- Guides for Educators. Available at [https://www.nrcs.usda.gov/Internet/FSE\\_DOCUMENTS/nrcs142p2\\_053280.pdf](https://www.nrcs.usda.gov/Internet/FSE_DOCUMENTS/nrcs142p2_053280.pdf) Accessed 30 Sept 2020
- Weng YL, Gong P, Zhu ZL (2008) Reflectance spectroscopy for the assessment of soil salt content in soils of the Yellow River Delta of China. *Int J Remote Sens* 29(19):5511–5531. <https://doi.org/10.1080/01431160801930248>
- Wu JW, Vincent B, Yang JZ, Bouarfa S, Vidal A (2008) Remote sensing monitoring of changes in soil salinity: a case study in Inner Mongolia, China. *Sensors* 8(11):7035–7049. <https://doi.org/10.3390/s8117035>
- Zhang M, Wang H, Pang X, Liu H, Wang Q (2017) Characteristics of soil salinity in the typical area of Yellow River Delta and its control measures. In *IOP Conference Series: Earth and Environmental Science* 64(1):012078. <https://doi.org/10.1002/ldr.1071>